ACS APPLIED MATERIALS & INTERFACES

Research Article

www.acsami.org

Oligonucleotides—Assembled Au Nanorod-Assisted Cancer Photothermal Ablation and Combination Chemotherapy with Targeted Dual-Drug Delivery of Doxorubicin and Cisplatin Prodrug

Vijayakumar Shanmugam,[†,∥] Yi-Hsin Chien,[†,∥] Yu-Sheng Cheng,[†] Tzu-Yu Liu,[†] Chih-Chia Huang,[‡] Chia-Hao Su,[§] Yu-Sen Chen,[⊥] Umesh Kumar,[⊥] Hua-Fen Hsu,*[,⊥] and Chen-Sheng Yeh*[,†]

[†]Department of Chemistry, Center for Micro/Nano Science and Technology, and Advanced Optoelectronic Technology Center, National Cheng Kung University, Tainan 701, Taiwan

[‡]Department of Applied Chemistry, National University of Kaohsiung, Kaohsiung 811, Taiwan

[§]Center for Translational Research in Biomedical Sciences, Kaohsiung Chang Gung Memorial Hospital, Kaohsiung 833, Taiwan

[⊥]Department of Chemistry, National Cheng Kung University, Tainan 701, Taiwan

Supporting Information

ABSTRACT: External stimuli responsive dual drugs carrier was synthesized with Au nanorods (NRs) as the platform. On Au NRs, single stranded DNAs were assembled using 5′ thiol end. Following this, complementary DNA (cDNA) strands were hybridized. This hybridized double stranded DNA facilitated doxorubicin (Dox) intercalation into the duplexes. The cDNA designed with the 5′ amine functional group assisted to tether platinum [Pt(IV)] prodrugs by establishing amide bond with the acid group at the axial ligand. The other axial acid group in Pt(IV) prodrugs was conjugated with the folic acid (FA) to target folate receptors overexpressed in the cancer cells. This targeting vehicle provided remote-controlled delivery of this high toxic cargo cocktail at the tumor site, ensuring extra specificity that can avoid acute toxicity, where release of Dox and Pt(IV) was achieved upon NIR 808 nm diode laser irradiation. The dehybridization set the Dox free to bind the cell nucleus and cellular reductants reduced Pt(IV) to yield toxic Pt(II), becoming an active drug. The in vitro and in vivo studies revealed that this external stimulus responsive combination drug delivery was significantly effective.

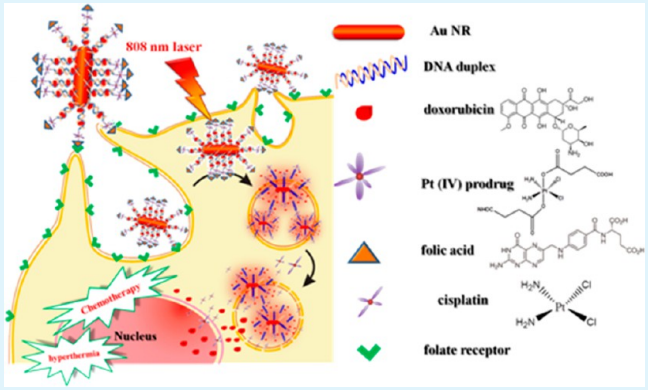

KEYWORDS: *Combination chemotherapy, dual drug delivery, photothermal ablation, hyperthermia, Au nanorod*

INTRODUCTION

In severe and advanced tumors, combined drug chemotherapy is gaining importance, which has already been proven to be clinically successful.[1−7] Cancer stem cells that are diagnosed pose a new challenge to existing chemotherapy and radiation therapies, as they are intrinsically resistant by being inactive or adopting a drug efflux mechanism or enhanced antiapoptotic protein and DNA repairing ability.[8] Hence to treat/cure this, drug combinations are explored. In contrast to single drug chemotherapy, the combined drugs treatment may show additive or synergistic or antagonistic effects. The pharmacokinetics shows potentiative or reductive responses with reference to the choice of drugs combination.[2] For example, endometrial cancer caused by the hormonal secretion is most common women malignancy in developed countries. In chemotherapy, doxorubicin (Dox) and cisplatin were identified as the active agents. Combining both agents have shown the increased response rate in phase III clinical trials.[4,5] Cytotoxic chemotherapy is an established modality for advanced breast cancer. The treatment of advanced breast cancer using paclitaxel and cisplatin drug combinations indicated a high efficacy in overall response rate.[6] Last, but not least, the combination of epirubicin plus cisplatin is an effective treatment for ovarian cancer.[7] Hence in the expedition to control the severity of the tumor, clinicians are coming out with these kinds of magic drug cocktails. Nevertheless, their enhanced treatment efficiency on tumor tissue has recorded toxicity to other tissues, forcing researchers to compromise for lower dosages. Because the cancer drugs have a wide spectrum of cytotoxicity, generally its nonspecific accumulation should be addressed to avoid any possible side effects. Therefore, the combined chemotherapy strongly demands an efficient delivery vehicle that can carry multiple cargos to the target site with less accumulation in the nontarget site so that the trade-off on

Received: January 6, 2014
Accepted: February 22, 2014
Published: February 22, 2014

dosage amount can be brought closer. The adoption of a nanocarrier could greatly minimize side effects of anticancer drugs besides their therapeutic efficacy.[9−11]

Combination chemotherapy using nanoscale delivery systems has hardly been reported. Only a few reports are on combined drug delivery through polymer encapsulated nanoparticles.[12−16] Nguyen and co-workers used a polymer-lipid hybrid nanocarrier to simultaneously deliver Dox and cisplatin.[12] The Dox was encapsulated into the liposome that was caged with cholesterol terminated poly acrylic acid with a cross-linker. This link is chosen to release the drug in the acid environment. The carboxyl groups in the surface were tethered with the cisplatin prodrug. Farokhzad and co-workers developed a poly(D,L-lactic acid-*co*-glycoli acid)-block-poly(ethyleneglycol) (PLGA-PEG) nanoparticles to carry cisplatin and docetaxel.[13] A polylactide derivative with reactive hydroxyl protrusion was employed to tether cisplatin prodrug by ester bonding, which can set free the drug in the cell. Nanoprecipitation of hydrophobic docetaxel was conducted by encapsulating with the di-block copolymer PLGA-PEG.

The combination chemotherapy mentioned above is formulated by polymer encapsulation. Hence the report of remote controlled delivery of combination chemotherapy in an inorganic nanoplatform is not yet developed. The nanocarrier that could release drug cargos in response to the external stimulus is more preferred in this extremely cell destructive combination chemotherapy. In this study, we used photothermal converter Au nanorods (NRs) as delivery vehicles to demonstrate near-infrared (NIR) triggered simultaneous photothermal ablation and combination chemotherapy in vitro and in vivo. On this platform, single stranded DNAs (ssDNAs) with 5′ thiol ends were assembled by thiol conjugation on the Au NRs; following this, the complementary DNA (cDNA) strands were hybridized. This hybridized double stranded DNA functioned as the Dox binder through intercalation of Dox into CG base pairs of a DNA duplex.[17−19]

The complementary cDNA was designed with a 5′ amine functional group to tether platinum(IV) [Pt(IV)] prodrugs by establishing an amide bond with the acid group in the axial ligand. The other axial acid group in Pt(IV) was conjugated with the folic acid (FA) to target folate receptors overexpressed in the cancer cells (Scheme 1). Pt(IV) prodrug is known to be inert, giving fewer side effects, relative to Pt(II) compounds. Upon entering cells, the Au NRs were exposed to a NIR diode laser to provide hyperthermia and drug release of Dox and the Pt(IV) prodrug. The Pt(IV) prodrugs were then reduced by cellular reductants to yield a toxic Pt(II) species. This targeting vehicle provides remote-controlled delivery of this high toxic cargo cocktail at the tumor site, ensuring extra specificity that can avoid acute toxicity, where release of Dox and Pt(IV) was achieved only upon NIR irradiation.

Scheme 1. (a) Dox/Pt(IV) Loading and Folic Acid Conjugation on dsDNA−Au NRs. (b) Targeting Drugs, Laser Stimulated Dehybridization, Drugs Release and Hyperthermia; the Released Pt(IV) Prodrugs Were Reduced Inside the Cancer Cells to Form Cytotoxic Pt(II) Complexes

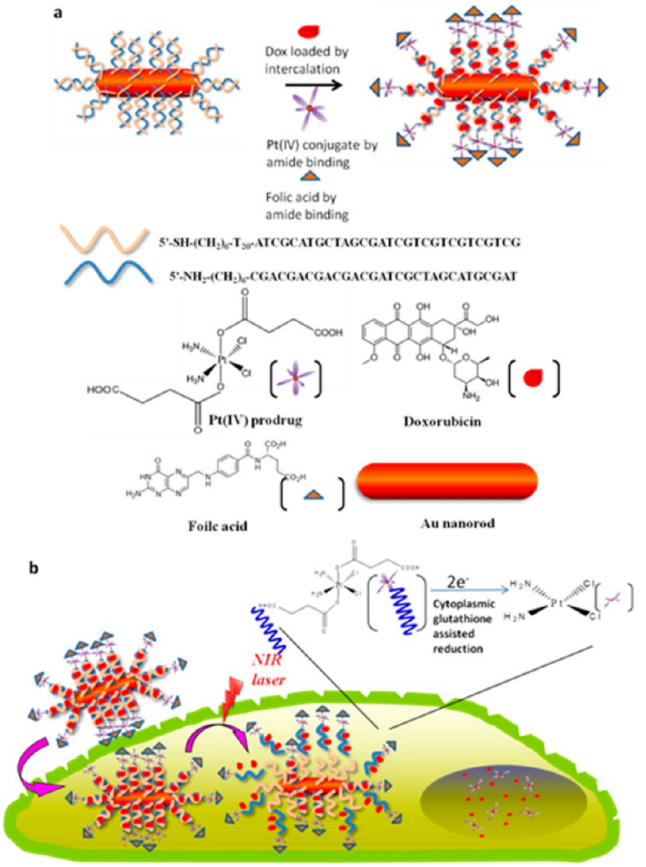

MATERIALS AND METHODS

Materials. All reagents were of analytical purity and used without further purification: hydrogen tetrachloroaurate trihydrate ($HAuCl_4$ $3H_2O$, 99%, Alfa Aesar), silver nitrate ($AgNO_3$, 99%, SHOWA), cetyltrimethylammonium bromide (CTAB, 99%, Sigma), L(+)-Ascorbic acid (Vitamin C, 99%, Riedel-de Haën), sodium borohydride ($NaBH_4$, 99%, Sigma), monopotassium phosphate (KH_2PO_4, 99%, J. T. Baker), dipotassium phosphate (K_2HPO_4, 100%, J. T. Baker), sodium chloride (NaCl, 99%, J. T. Baker), sodium dodecyl sulfate (SDS, 100%, J. T. Baker), Doxorubicin hydrochloride (Dox, 98%, Acros), oligonucleotide and thiolated oligonucleotide (MDBio, Inc.), *cis*-diamminedichloro-platinum(II) ($Pt(NH_3)_2Cl_2$, 99.9+%, ALDRICH), succinic anhydride ($C_4H_4O_3$, 99%, ALFA), *N*,*N*-dimethylformamide ($HCON(CH_3)_2$, 100%, Mallinckrodt), and ethanol (C_2H_2OH, 99.9%, J. T. Baker)

Gold Nanorods (Au NRs) Synthesis. Au NRs with an aspect ratio of ∼4 were prepared using a seedless growth method. Typically, 120 μL of $AgNO_3$ (0.1 M) was added to 100 mL of 0.5 mM $HAuCl_4$ solution containing 0.1 M CTAB and allowed to vigorously stir for 5 min. We then added 0.6 mL of 0.1 M ascorbic acid to reduce Au(III) to Au(I). Immediately after this, 40 μL of $NaBH_4$ solution (0.1 M) was injected and the solution was kept stirring for 2 h. The product was collected by centrifugation at 10,000 rpm. The atomic concentration of AuNRs was quantified by an inductively coupled plasma-atomic emission spectrometer (ICP-AES, Jobin Yvon JY138 spectroanalzer).

Preparation of DNA Duplex-Modified AuNRs. We first functionalized single DNA strands with 5′ thiol (SH-5′-$(CH_2)_6$-T20-ATCGCATGCTAGCGATCGTCGTCGTCGTCG (T20-ssDNA)) onto Au NRs surface through a protocol[20] similar to that used in DNA immobilization on spherical Au. We incubated 3.6 nM Au NRs with thiolated T20-ssDNA in ∼2430/1 of T20-ssDNA/Au NRs molar ratio, followed by sonication for ∼15 s at every 10 min interval for 1 h, and then continued with vortexing for 23 h. Sodium dodecyl sulfate (SDS) was subsequently added to bring the final concentration

dx.doi.org/10.1021/am5000905 | ACS Appl. Mater. Interfaces 2014, 6, 4382−4393

to 0.015% (SDS), stabilizing the NRs for further salting. To facilitate the attachment of DNA by reducing the electrostatic repulsion between the immobilized DNA and the residual DNA left in solution, 10 aliquots of 2.5 M NaCl/10 mM phosphate buffer (PBS) were added stepwise into the mixture to produce the final concentration of 0.5 M NaCl at 55 °C. The mixtures were vortexed at room temperature for another 14 h and then washed with 0.1 M NaCl/PBS (pH 7.0) to remove unbound DNA. The T20-ssDNA-modified NRs were then hybridized with the complementary DNA strands cDNA; 5′-NH_2-$(CH_2)_6$-CGACGACGACGACGATCGCTAGCATGCGAT in 0.15 M NaCl/PBS (pH 7.0) containing 0.05% SDS at 80 °C for 2 min, followed by 1 day of vortexing at room temperature. The synthesized dsDNA−Au NRs were washed using 0.15 M NaCl/PBS at 28 °C and collected through 15,000 rpm centrifugation to remove unspecific binding duplexes. The amount of immobilized T20-ssDNA and duplex was estimated with fluorescence-based quantization using FAM-labeled T20-ssDNA as reported in previous studies.[21]

Synthesis and Characteriasation of Cisplatin Prodrugs. *cis*,*cis*,*trans*-diamminedichlorodihydroxy-platinum(IV) ($Pt(NH_3)_2Cl_2(OH)_2$ (DHP)) and *cis*,*cis*,*trans*-diamminedichlorodisuccinato-platinum(IV) ($Pt(NH_3)_2Cl_2(OOCCH_2CH_2CO_2H)_2$ (DSP)) were prepared according to the reported procedures.[22,23] Briefly, a mixture of *cis*-$Pt(NH_3)_2Cl_2$ (1g, 3.34 mmol) and H_2O_2 (30 wt %, 35 mL, 30 mmol) in 25 mL of H_2O was heated at 50 °C and stirred for 1 h. After 1 h, the light yellow solution was cooled to the room temperature and its volume was reduced in vacuo. A pale yellow solid of DHP was crystallized. The product was collected via vacuum filtration, washed with ice cold H_2O and diethyl ether, and vacuum dried. Yield: 0.7841 g (70.7%). A mixture of *cis*,*cis*,*trans*-$Pt(NH_3)_2Cl_2(OH)_2$ (DHP; 0.7790 g, 2.33 mmol) and succinic acid anhydride (0.9326 g, 9.32 mmol) in 10 mL of DMSO was heated at 70 °C and stirred for 15 h to give a light yellow solution. The light yellow solution was cooled and the volume of solvent was reduced via lyophilization. The actone was added to give a pale yellow solid of DSP at −20 °C. The product was collected via vacuum filtration, washed with cold diethyl ether, and vacuum dried. Yield: 0.6711 g (54%). ESI-MS calculated for $[M - H]^-$ m/z 531.98, found 531.98. ^{1}H NMR of DSP (d_6-DMSO, 400 MHz, δ ppm): 2.33 (m, $-CH_2-$), 2.46 (m, $-CH_2-$), 6.46 (s, $-NH_3$), 12.07 (s, −COOH).

Synthesis of Pt(IV)−dsDNA−Au NRs. One milliliter of 280 ppm dsDNA−AuNRs from the above process was added with 16.56 mM of 100 μL EDC and NHS, respectively, so that a 1:219:262:262 molar ratio of AuNR:Pt(IV) prodrug:NHS:EDC was maintained. This mixture was vortexed for 120 min. Then the conjugates were washed twice with 0.15 M NaCl/PBS (pH 7). Following centrifugation, the precipitates were dispersed in 0.15 M NaCl/PBS (pH 7).

Electrochemical Analysis. Electrochemical measurements were performed in a CH instrument with chi6142c software, having a three electrode system with glassy carbon as working, platinum as counter, and Ag/AgCl as the reference electrode. The cyclic voltograms of 5 mM prodrug dissolved in PBS buffer of 0.1 M KCl with different pH (7.4 and 6) were recorded at 50, 100, 150, 200, 250, 300, 350, and 400 mV s^{-1} scan rates.

Folic Acid Conjugation on Pt(IV)−dsDNA−Au NRs. 2000 ppm of 20 μL Pt(IV)−dsDNA−Au NRs diluted in 920 μL of a DMSO/PBS mixture was added with 10 μM of 30 μL of FA and 2 mM of 15 μL of EDC/NHS and then vortexed for 4 h. Then the materials were washed 3 times with 0.15 M NaCl/PBS. Following centrifugation, the pellets were dispersed in 0.15 M NaCl/PBS.

Loading Dox into DNA Duplex on FA−Pt(IV)−dsDNA−Au NRs. 42.05 μM of Dox was mixed with FA−Pt(IV)−dsDNA−Au NRs at room temperature for 24 h. The conjugates were washed 3 times with 0.15 M NaCl/PBS (pH 7.0) accompanied by centrifugation at 15,000 rpm to remove unbound Dox. The fluorescence emission at 585 nm (with excitation at 480 nm) of unbound Dox in the supernatant following each centrifugation was measured with a fluorescence spectrophotometer (F-2500; Hitachi Koki Co., Ltd., Tokyo, Japan). A standard linear calibration curve was performed to calculate the corresponding amount of unbound Dox. The associated Dox was obtained by subtracting the unbound Dox from the original Dox dose. The conjugates were then redispersed in 0.15 M NaCl/PBS (pH 7.0) and stored at 4 °C for further experiments.

Au NRs and Their Conjugates Characterization. Absorbance profiles of the Au NRs and DNA-modified Au NRs were obtained from a UV−vis spectrophotometer (8452A; Hewlett-Packard Company, Palo Alto, CA). The electron micrographs were taken with transmission electron microscopes (JEOL 3010 at 300 KV and PHILIPS CM-200 at 200 KV) and the ζ-potential was measured with a Zetasizer analyzer (Malvern, U.K.). Elemental composition was analysed using inductively coupled plasma (ICP) spectroanalyzer (Jobin Yvon JY138). For the ICP analysis, nanostructures were digested in aqua regia. Fluorescence was obtained using a Fluoromax-4 Spectrofluorometer (Horiba Scientific). The quantification of cell viability was done using an ELISA plate reader (Thermo Scientific Multiskan EX).

Stability Test for Pt(IV)−dsDNA−Au NRs. The Pt(IV) released without laser stimuli from 50 ppm of Pt(IV)−dsDNA−Au NRs dispersed in 0.15 M NaCl/PBS (pH 7) was monitored for 24 h at the 2, 4, 6, and 24 interval each, kept at 37 °C. For this observation, aliquot was centrifuged and the concentration of the Pt was measured with ICP from the supernatants.

Stability Test for Dox−dsDNA−Au NRs. The Dox released without laser stimuli from 50 ppm of Dox−dsDNA−Au NRs dispersed in 0.15 M NaCl/PBS (pH 7) was monitored for 24 h at the 2,4, 6, and 24 h interval each, kept at 37 °C. For this observation, aliquot was centrifuged and the fluorescence intensity of the supernatants was measured at 585 nm for Dox. It is noted that the fluorescence emission of Dox molecules is sensitive to the presence of DNA in solution. The intercalation into the DNA duplex quenching Dox fluorescence as well as the dehybridized cDNA could also decrease the emission intensity of Dox. Therefore, the quench effect of the liberated Dox needs to be taken into account. Thus, the actual released Dox was calculated from a linear calibration curve (fluorescence intensity vs concentration) based on the Dox fluorescence drawn from the Dox + cDNA (physical mix) solution, where the amount of cDNA corresponds to the liberated ∼2.9% quantity. This calibration approach with consideration of the liberated cDNA was used to quantify Dox.

Temperature Elevation Profile by Photothermal Conversion. Concentration dependent temperature elevation was monitored with 50, 100, and 200 ppm dsDNA−Au NRs in 0.15 M NaCl/PBS (pH 7.0) to 96-well plates at a fixed laser power of 3 W/cm^2 using a near-infrared (NIR) diode laser (808 nm). Following this, at fixed concentration of 200 ppm

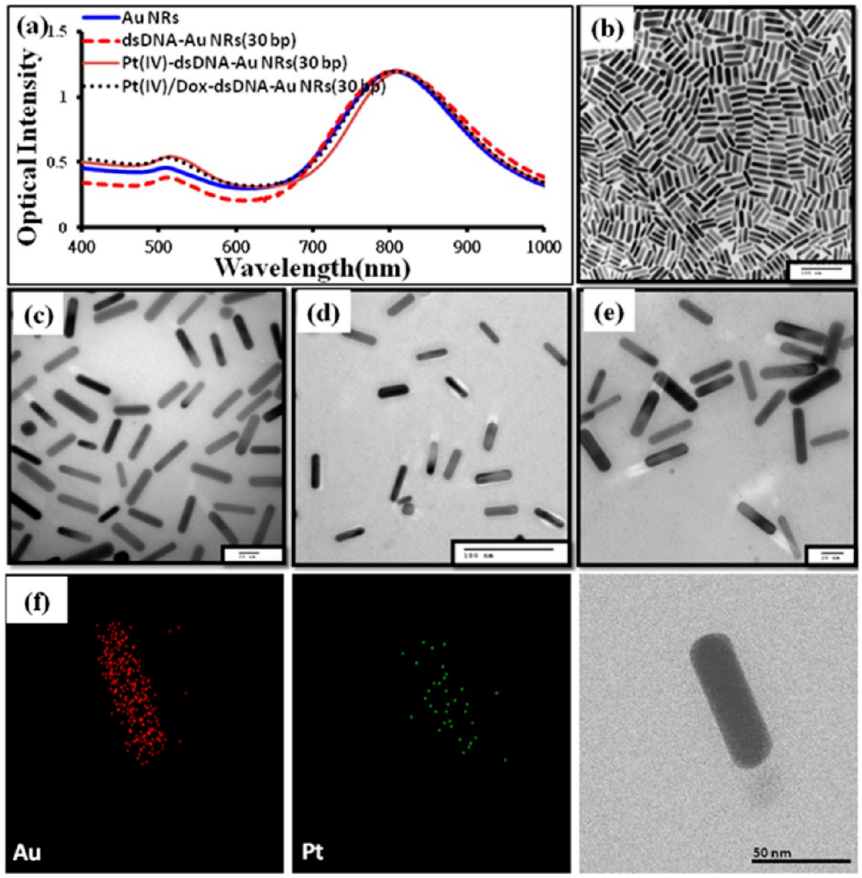

Figure 1. (a) UV−vis absorbance of Au NRs, dsDNA−Au NRs, Pt(IV)−dsDNA−Au NRs, and Pt(IV)/Dox−dsDNA−Au NRs. TEM images of (b) Au NRs, (c) dsDNA−Au NRs, (d) Pt(IV)−dsDNA−Au NRs, and (e) Pt(IV)/Dox−dsDNA−Au NRs. DNA sequence has 30 base pairs. (f-row) Elemental maps of Pt(IV)/Dox−dsDNA−Au NRs showing Au in red, Pt in green, and the corresponding TEM image.

dsDNA−Au NRs the efficiency of photoinduced temperature increase of the solution was investigated under various irradiation power of 1.3, 2, 3, and 4 W/cm^2 for 10 min of irradiation. The well was exposed to the laser light with a focused area of 0.15 cm^2. The change in solution temperature was determined by digital thermometer (TES 1319A−K type).

In Vitro Release of DNA Upon Laser Stimulation. For the DNA release studies, the complementary FAM-labeled DNAs were hybridized with ssDNA−Au NRs. 100 μL of the above Au NRs was illuminated with 1.5 W/cm^2 laser for 10 min ON, followed by 30 min with the laser OFF. The FAM fluorescence intensity from the released cDNA was evaluated from the supernatants after centrifugation, and then using a calibration curve the cDNA release was quantified.

In Vitro Release of Pt(IV) Upon Laser Stimulation. For the Pt(IV) release studies, 100 μL of 50 ppm Pt(IV)−dsDNA−Au NRs was illuminated with 1.5 W/cm^2 laser for 10 min ON, followed by 30 min with the laster OFF for three consecutive sequences. The aliquots were centrifuged and the concentration of the Pt was measured with ICP from the supernatants.

In Vitro Release of Dox Upon Laser Stimulation. For the Dox release studies, 100 μL of 50 ppm Dox-dsDNA-Au NRs was illuminated with 1.5 W/cm^2 laser for 10 min ON, followed by 30 min of laser OFF for three consecutive sequence. The aliquots were centrifuged and the Dox fluorescence intensity was documented to measure the liberated Dox from the supernatants, and then followed a calibration procedure to quantify Dox.

Fluorescence Examination by the Confocal Microscope. 1.2 × 104 HeLa cells were grown in 8-well chamber slides for 24 h. Then this medium was exchanged with 200 ppm of FA−Pt(IV)/Dox−dsDNA−Au NRs. The cells were incubated in this medium for 2 h; after this, the medium was removed and the cells were washed with PBS 2 times for the sequential addition of fresh medium. For laser illumination, these cells were immediately exposed to a diode NIR laser (808 nm) for 10 min. Following this, the cells were incubated for different periods. Finally, the cells were rinsed 2 times and 165 μL of 4% paraformaldehyde was added to fix the cells. The cell membrane was stained with Alexa488 for green flourescence. The nuclei were counter stained with DAPI dye prior to examination. Fluorescence images for the prepared slides were taken with a Nicon Confocal Microscope System (ECLIPSE Ti series, NIKON).

Quantitative Cell Viability with MTT Assay Evaluation. 8 × 10^3 HeLa cells/well were cultured on 96-well plates for 24 h, followed by the treatment of the materials. After 2 h of incubation, the cells were washed 2 times with PBS and fed with fresh medium. For laser illumination, the cells were subjected to 3 W/cm^2 of NIR laser irradiation for 10 min. The cells were then incubated for another 24 h. For the cytotoxicity analysis, the medium containing 10% MTT reagent was added and the cultures were incubated for 4 h to allow formazan dye to form. After this, the MTT medium was removed, dimethyl sulfoxide (DMSO) was added as a solvent, and cell viability was

calculated based on the absorbance of purple formazan, which is measured using an ELISA plate reader.

Tumor-Bearing Animal Model. The HeLa cells were maintained in DMEM (GIBCO, Taiwan). The medium was supplemented with 10% fetal bovine serum (FBS; GIBCO, Taiwan) and penicillin−streptomycin (100 μg/mL). The cell line was incubated at 37 °C with 5% CO_2 in air. The cells were trypsinized from the tissue culture flasks and washed 2 times with PBS, and were then counted on a hemacytometer slide and resuspended in serum-free, antibiotic-free normal saline before injection. The male nude mice (6 weeks old) were provided by the National Cheng Kung University (NCKU) Laboratory Animal Center (Tainan, Taiwan). All animals received humane care in compliance with NCKU guidelines for the maintenance and use of laboratory animals in research. All of the experimental protocols involving live animals were reviewed and approved by the Animal Experimentation Committee of NCKU. The HeLa tumor xenografts were established through a subcutaneous dorsal flank injection of 106 tumor cells in 100 μL of normal saline by using a 27G needle. A visible tumor, usually observed 1 week after implantation, was ready for studies. The tumor size was measured along the longest width and the corresponding perpendicular length. The tumor volume was calculated using the volume of an ellipsoid, where volume = $4\pi/3$ (length/2 × width/2 × depth/2). This study assumed that depth = width and $\pi = 3$, resulting in volume = 1/2 × length × $(\text{width})^2$. Prior to respective treatment, the animals were anesthetized using 2% isoflurane (Abbott Laboratories, Abbott Park, IL) mixed with 100% O_2 and delivered using a veterinary anesthesia delivery system (ADS 1000; Engler Engineering Corp., Hialeah, FL).

RESULTS AND DISCUSSION

Synthesis and Characterization of Au NRs Carrying Dox and Pt(IV) Prodrug. To formulate the FA targeted Au NRs carrying Dox and Pt(IV) vehicles, the surface conjugation of Au NRs followed a preparation sequence of DNA duplex → Pt(IV) prodrug → FA → Dox intercalation. In a typical preparation, Au NRs with an average aspect ratio of 4 were prepared using seedless growth method[24] with slight modifications. AuNRs with an average length and width of ~38.5 and ~9.5 nm, respectively, measured from transmission electron microscopy (TEM), were dispersed in H_2O and showed typical longitudinal SPR band maxima at 808 nm (Figure 1a,b). Single strand DNAs (30 base pairs) with 5′thiol (SH-5′-$(CH_2)_6$-T20-ATCGCATGCTAGCGATCGTCGTCG-TCGTCG) were conjugated on the surface of NRs. The spacer T20 in the DNA sequence was used to reduce steric hindrance during hybridization. The complementary strands (cDNA; TAGCGTACGATCGCTAGCAGCAGCAGC-$(CH_2)_6$-NH_2-5′) were introduced to hybridize with the ssDNA to form duplex on the NRs surface (dsDNA−Au NRs) in PBS. The SPR bands and morphology were well preserved in dsDNA−Au NRs with hydrodynamic diameter of ~72 ± 9 nm, determined by Dynamic Light Scattering (DLS) (Figure 1a,c). The dsDNA−Au NRs were able to disperse in 0.15 M NaCl/PBS (pH 7.0). It is noted that the absorbance profile of Au NRs became broaden in the same 0.15 M NaCl/PBS (pH 7.0) due to occurrence of NRs aggregation. The quantification of the immobilized duplex DNA was performed with fluorescence-based method using FAM-labeled DNA (FAM: 6-carboxy-fluorescine; TAGCGTACGATCGCTAGCAGCAGCAGCA-GC-5′-FAM). The amount of immobilization was measured

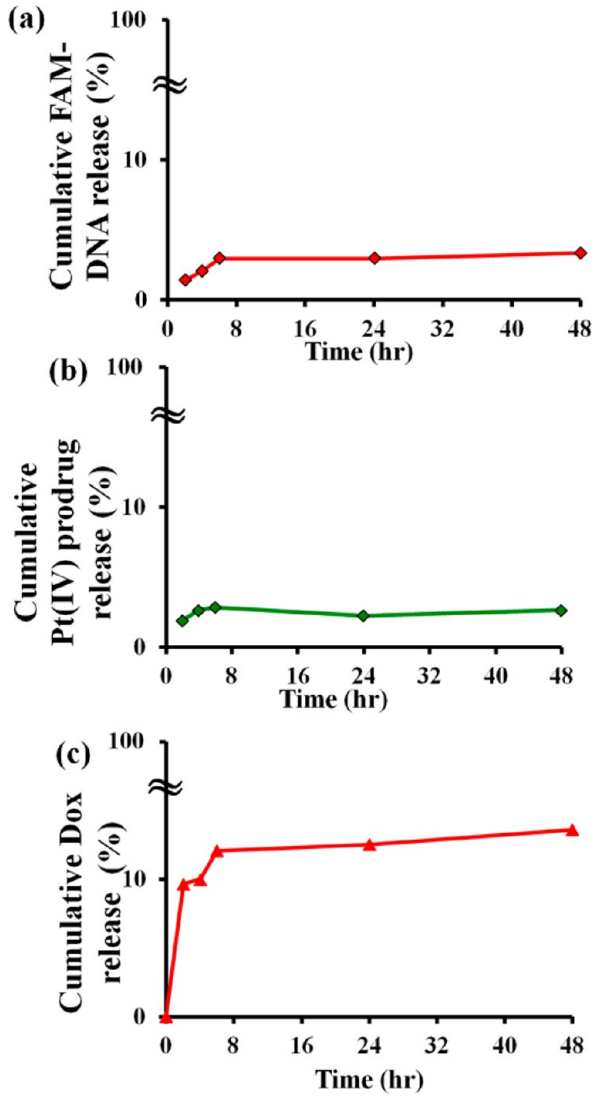

Figure 2. (a) Time-dependent stability of duplex on dsDNA−Au NRs measured by using FAM-labeled complementary DNA. FAM-labeled cDNA release without laser stimuli was monitored periodically at 2, 4, 6, 24, and 48 h from 50 ppm (based on Au ion concentration) of dsDNA−Au NRs dispersed in 0.15 M NaCl/PBS (pH 7.0) at 37 °C by measuring the fluorescence of FAM-labeled cDNA released in the supernatants. (b) Stability of Pt(IV) in Pt(IV)−dsDNA−Au NRs. Pt(IV) release without laser stimuli was monitored periodically at 2, 4, 6, 24, and 48 h from 50 ppm (based on Au ion concentration) of Pt(IV)−dsDNA−Au NRs dispersed in 0.15 M NaCl/PBS (pH 7.0) at 37 °C by measuring the Pt concentration in the supernatants through ICP measurements. (c) Stability of Dox in Dox−dsDNA−Au NRs. Dox release without laser stimuli was monitored periodically at 2, 4, 6, 24, and 48 h from 50 ppm (based on Au ion concentration) of Dox−dsDNA−Au NRs in 0.15 M NaCl/PBS (pH 7.0) at 37 °C by measuring the Dox fluorescence. An early stage burst release of ~12% was observed at 37 °C in the initial 6 h and reached a static position till the end of 24 h.

from the decrease of fluorescence intensity of FAM-labeled DNA left in supernatants and calculated based on a calibration curve according to FAM-labeled DNA concentration. It was quantified to be 64 duplexes per NR on an average.

The cDNA with a 5′ amine end was chosen to hybridize complementary DNA thiolated on Au NRs. The presence of the amine group provided an opportunity for us to establish

dx.doi.org/10.1021/am5000905 | ACS Appl. Mater. Interfaces 2014, 6, 4382−4393

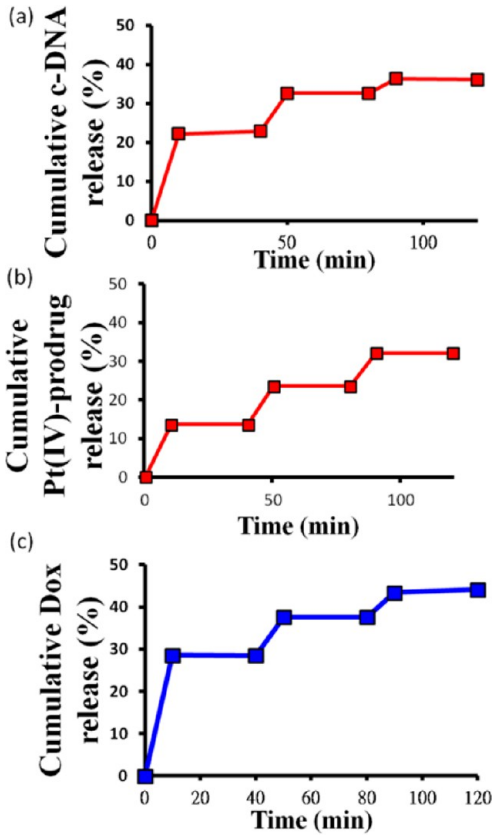

Figure 3. (a) Effect of laser illumination on FAM-labeled cDNA release from dsDNA–Au NRs (50 ppm; Au ion concentration). Laser stimulation with 1.5 W/cm^2 followed a sequence of three ON/OFF laser pulses with 10 min ON duration and 30 min OFF. The fluorescence from the released FAM-labeled cDNA was quantified. (b) Effect of laser stimulation on Pt(IV) prodrugs release from Pt(IV)–dsDNA–Au NRs (50 ppm; Au ion concentration). Laser stimulation with 1.5 W/cm^2 followed a sequence of three ON/OFF laser pulses with 10 min ON duration and 30 min OFF. The Pt(IV) prodrugs release was collected from supernatants by centrifugation of solutions, and then subjected to ICP measurements. (c) Effect of laser stimulation on Dox release from Dox–dsDNA–Au NRs (50 ppm; Au ion concentration). Laser stimulation with 1.5 W/cm^2 followed a sequence of three ON/OFF laser pulses with 10 min ON duration and 30 min OFF. The fluorescence of the released Dox was quantified before and after the laser stimulation in the consecutive ON/OFF sequences.

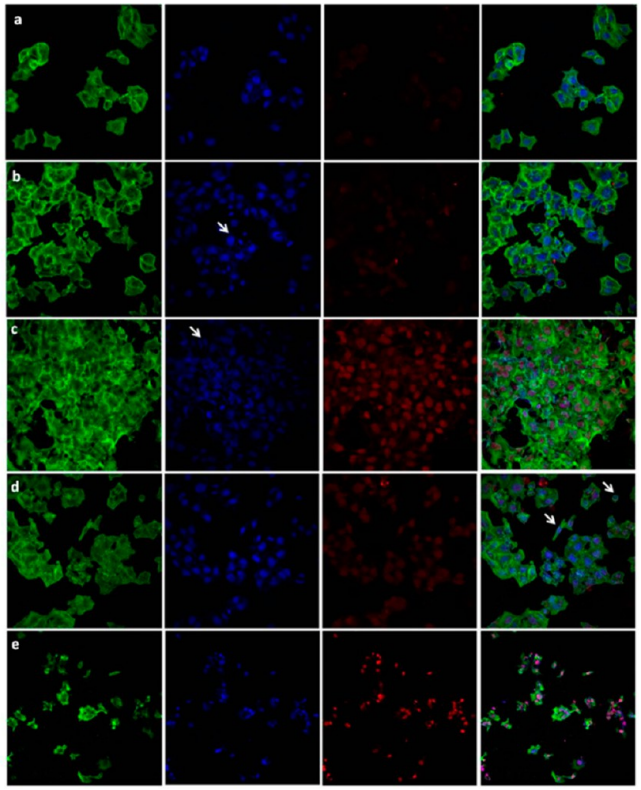

Figure 4. Confocal images of the HeLa cells incubated with 200 ppm FA–Pt(IV)/Dox–dsDNA–Au NRs and followed by irradiation with 808 nm CW diode laser of 1.3 and 3 W/cm^2 for 10 min. (a) Cells incubated with the nanomaterials for 2 h without exposure of laser irradiation. (b) Cells incubated with the nanomaterials for 2 h, and then exposed to 1.3 W/cm^2 laser power irradiated. The image was taken immediately after laser exposure (c) content of panel b incubated for an additional 24 h after the laser irradiation (the arrows in panels b and c represent the cells with intact and hazy nucleus, respectively). (d) Cells incubated with the nanomaterials for 2 h, and then exposed to 3 W/cm^2 laser power. The image was taken immediately after laser exposure (the arrows represent the cells with severe cell membrane damage). (e) content of panel d incubated for an additional 24 h after the laser irradiation (red fluorescence, released Dox; green fluorescence, cell membrane stained with Alexa 488; blue fluorescence, nucleus stained with DAPI).

additional drug payload, carrying Pt(IV) prodrugs via amide linkage. We synthesized Pt(IV) prodrugs, *cis,cis,trans*-Pt-$(NH_3)_2Cl_2(OOCCH_2CH_2CO_2H)_2$ (DSP: *cis,cis,trans*-diamminedichlorodisuccinato-platinum(IV)) by the incorporation of succinic acid into the axial position of *cis,cis,trans*-Pt-$(NH_3)_2Cl_2(OH)_2$ (DHP: *cis,cis,trans*-diamminedichlorodihydroxy-platium(IV)). The Pt(IV) prodrugs (DSP) were confirmed with ESI-MS and ^{1}H NMR spectra, as shown in Figures S1 and S2 (Supporting Information), respectively. Electrochemical analysis provided the studies of Pt(IV) reduction to loss axial ligands. The reduction potential was measured at varied scan rates and derived by extrapolation of scan rates to 0 mV s^{-1}. The electrochemical behavior of Pt(IV) showed a positive shift in the reduction peak from −0.75 to −0.69 V, with the reduction in the pH from 7.4 to 6 (Figures S3 (Supporting Information) and 4), confirming the divalent formation. A similar positive shift in the scale with the change in pH aids to conclude that the acidic environment would catalyze the conversion of Pt(IV) to active Pt(II).[25] Conjugation of the cDNA chain on the axial ligand is not expected to significantly change the reduction potential of Pt(IV). To conjugate Pt(IV) prodrugs on dsDNA–Au NRs, the carboxylic groups in one of the axial ligands of Pt(IV) prodrugs formed amide linkage with dsDNA through (1-ethyl-3-(3-dimethylaminopropyl)carbodiimide hydrochloride/*n*-hydroxysuccinimide (EDC/NHS) reaction. The resulting Pt(IV)–dsDNA–Au NRs remained dispersed in 0.15 M NaCl/PBS (pH 7.0) (Figure 1d). The loading efficiency of Pt(IV) prodrugs in each NR was calculated by subtraction of the Pt concentration left in the supernatant that was measured by ICP from the total amount used for conjugation. The approximate Pt loading was estimated to be 63 Pt(IV) per dsDNA–Au NRs, which is consistent with the quantity of duplexes per NR. The laser induced photothermal effect on the surface of NRs was expected to dehybridize the duplex to release cDNA free in the endogenous medium. In this medium, the reductants, like glutathione or aspartate, can reduce Pt(IV) to Pt(II) active

dx.doi.org/10.1021/am5000905 | ACS Appl. Mater. Interfaces 2014, 6, 4382–4393

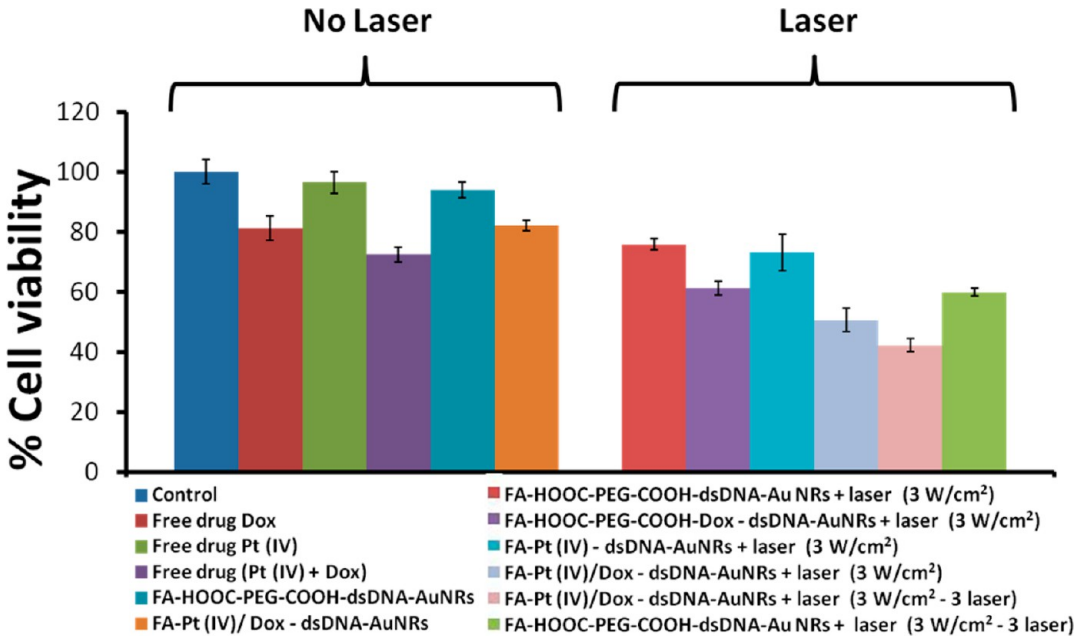

Figure 5. Cell viability of HeLa cells individually incubated in 200 ppm of FA−HOOC−PEG−COOH−dsDNA−Au NRs, FA−HOOC−PEG−COOH−Dox−dsDNA−Au NRs, FA−Pt(IV)−dsDNA−Au NRs, and FA−Pt(IV)/Dox−dsDNA−Au NRs and equivalent free drugs, which were same amount carried by Au NRs, with Dox (1.6 μM), Pt(IV) (0.16 μM), Pt(IV) (0.16) +Dox (1.6 μM). For the treatments with irradiation of 808 nm, CW diode laser of 3 W/cm^2 power density was illuminated for 10 min. 3W/cm^2 − 3 laser represents three cycles of ON/OFF laser pulses with 10 min ON duration and 30 min OFF.

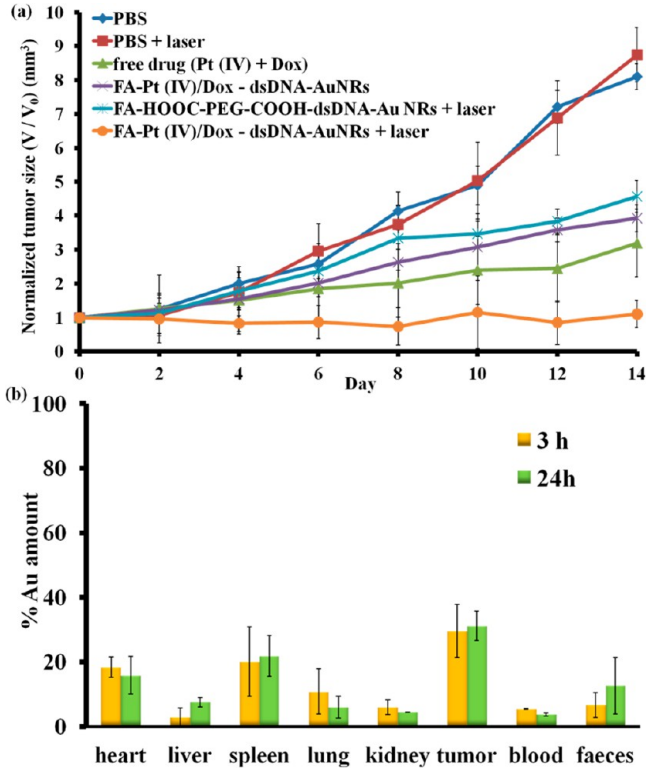

Figure 6. (a) Time dependent change in the HeLa tumor volume implanted in nude mice after different treatments. The tumor volume is plotted against the days of observation. Each group has a mice population of five. (b) Biodistribution of FA−Pt(IV)/Dox−dsDNA−Au NRs in different tissues of mice bearing HeLa tumors after 3 and 24 h of injection, expressed based on the Au ion concentration measured by ICP.

drug; simultaneously, the axial ligand cleavage also set them free from cDNA to act on the host DNA (nuclei). The active cisplatin will bind the host DNA to hamper the cell cycle. The acid group in the other axial ligand acts as the site to form another amide link with the amine group in the FA so that α- and γ-carboxylic groups can target the nanoparticles to the folate receptor over expressed tumor cells.[26] Folate targeting for this folic acid conjugation was carried on the folate over expressing HeLa cells in comparison to the non-folic acid conjugation that showed a 2-fold increase in the uptake after 4 h of incubation, based on the Au ion concentration measured by ICP.

Dox was loaded by intercalation to DNA duplexes of dsDNA−Au NRs. The nucleic bases of the DNA duplex are in the coplanar form, which allows the flat aromatic rings of the Dox molecules to intercalate into adjacent base pairs and are stabilized by electrostatic, dipole−dipole, dispersive interactions and $\pi-\pi$ stacking.[27,28] Additionally, this Dox loading was carried out at pH 7.0, a condition that facilitated a positive charge to the Dox molecule (p*K*a = 8.3),[29] which favored Dox to crowd around the DNA duplex via electrostatic attraction that enhanced intercalation. The TEM image of Dox-loaded Pt(IV)−dsDNA−Au NRs (Pt(IV)/Dox−dsDNA−Au NRs) without showing aggregation is shown in Figure 1e. The elemental maps shown in Figure 1f provide additional evidence for the presence of Au and Pt elements for the NRs. The amount of the loaded Dox was determined by measuring the fluorescence emission of Dox at 585 nm. Prior to the Dox quantification, the stability of the DNA was conducted, which is explained in a later part of our paper along with other drug stabilities, for the reader's easy follow-up. The fluorescence of unbound Dox in the supernatants was subtracted from the initial Dox fluorescence to get the Dox loading with standard calibration curve, which resulted in ∼580 Dox per Au NR. The consecutive −CG− base pairs are known to be the preferred

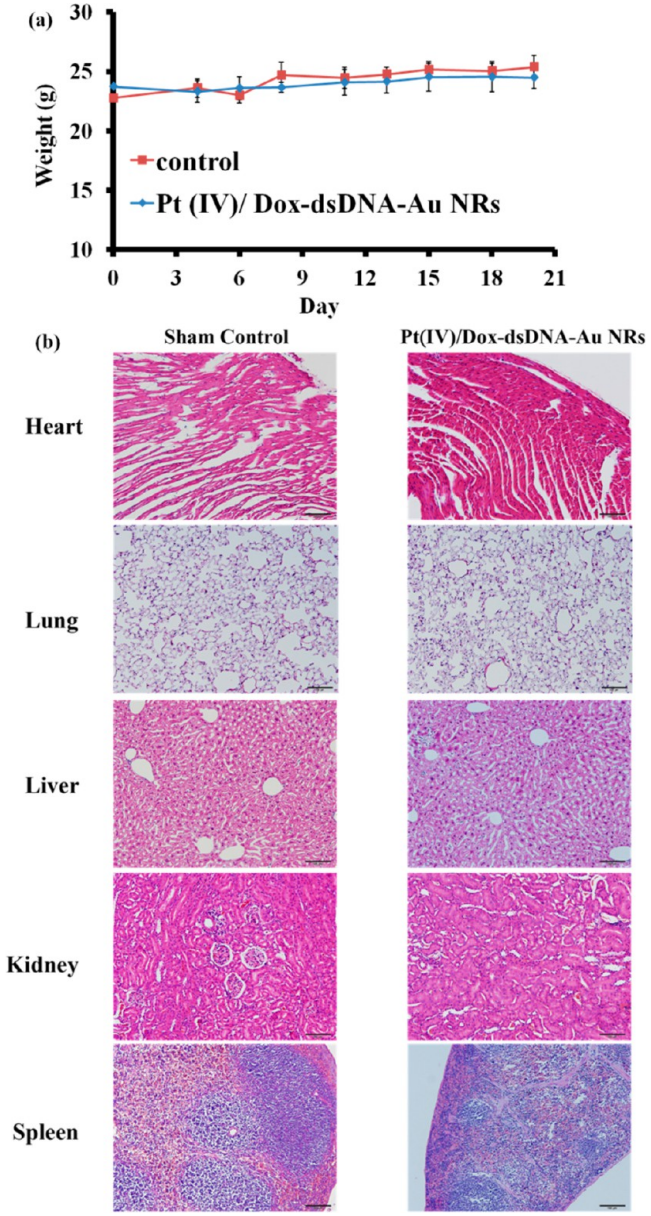

Figure 7. (a) Long term weight observation of the healthy mice (n = 7) injected with Pt(IV)/Dox−dsDNA−Au NRs at the Dox dosage of 2 mg/kg, revealing that the materials do not pose significant weight change. (b) The organ tissues (heart, lung, liver, kidney, and spleen) removed after 21 days of Pt(IV)/Dox−dsDNA−Au NRs injection to the healthy mice in comparison with control (PBS injection).

Dox binding sites.[17−19] On the basis of the sequences shown in Scheme 1, 10 Dox per duplex was expected, an ideal situation without considering steric factors. The experimental measurement indicated loading capacity of 9 Dox per duplex, which is consistent with the prediction (10 Dox per duplex). Another set of conjugation with 15 bp DNA duplexes (SH-5′-$(CH_2)_6$-T20-ATCGCATGCTAGCGA and TAGCGTACGATCGCT-$(CH_2)_6$-NH_2-5′) were prepared to demonstrate the flexibility of this design with the difference in sequence and eventually the drug loading. With 15 bp duplexes, 319 Dox were carried per Au NR that corresponded to 5 Dox per duplex. UV−vis absorbance and TEM images of the corresponding NRs were given in Figure S5 (Supporting Information).

Stability of dsDNA−Au NRs, Pt(IV)−dsDNA−Au NRs, and Dox−dsDNA−Au NRs. Prior to exposure to the CW diode laser (808 nm), we respectively evaluate the stability of dsDNA−Au NRs, Pt(IV)−dsDNA−Au NRs, and Dox−dsDNA−Au NRs. Hence the stability with release profile was studied for 48 h in PBS buffer at 37 °C. The FAM-labeled DNAs as the complementary strands were used for dsDNA−Au NRs to monitor the stability and showed a stable hybridization with only ∼3.3% liberated DNA after 48 h (Figure 2a). For the Pt(IV)−dsDNA−Au NRs, the Pt(IV) release from the conjugates was estimated with the inductively coupled plasma (ICP) spectrometer. At the 2, 4, 6, 24, and 48 h intervals, the solutions were centrifuged and the supernatants containing Pt were measured. The Pt(IV) release reached a maximum of ∼2.8% at 6 h, and then leveled off (Figure 2b). The ∼2.8% release is consistent with the liberation of DNA. Similarly, Dox−dsDNA−Au NRs was examined for the Dox release by measuring the Dox fluorescence intensity at 2, 4, 6, 24, and 48 h intervals. There was a 12% release in the initial 6 h; thereafter, no more additional release was observed (Figure 2c). It should be mentioned that the fluorescence emission of Dox molecules is sensitive to the presence of DNA in solution. The intercalation into the DNA duplex quenches Dox fluorescence (Figure S6, Supporting Information) as well as the dehybridized cDNA could also decrease the emission intensity of Dox. Therefore, the quench effect of the liberated Dox requires to be taken into account. Thus, the actual released Dox was calculated from a linear calibration curve (fluorescence intensity vs. concentration) based on the Dox fluorescence drawn from the Dox + cDNA (physical mix) solution, where the amount of cDNA corresponds to the liberated ∼3 % quantity. This calibration approach with consideration of the liberated cDNA was used to quantify Dox throughout the studies.

In Vitro Release Upon Laser Illumination. In the above design, both drugs' (Dox and Pt(IV)) release are controlled by an external laser trigger, whose energy will be translated to heat by Au NRs, which dehybridizes duplex DNA to release drugs. The NIR irradiation that is absorbed by the nanorod increases the local temperature; hence the thermosensitive DNA dehybridises and releases the complementary DNA strand. Eventually, the DOX loaded by intercalation and the Pt(IV) prodrug conjugated to the complementary strand will be released from the DOX/Pt(IV)−dsDNA−Au.[30] Hence the photothermal property of the synthesized Au NRs was investigated under 808 nm continuous wave diode laser. A thermocouple was used to measure the medium (0.15 M NaCl/PBS (pH 7.0)) temperature. The temperature of the medium increased as particle concentration and laser intensity increased (Figures S7 and S8, Supporting Information). Next, laser stimulated cDNA and drug release from the Au NRs was evaluated in a pulsatile release mode, which demonstrated precise control of cargo release with light ON. For the cDNA release in response to the NIR laser trigger, the cDNA with FAM fluorescence tag (FAM-labeled DNA) was used to form dsDNA−Au NRs. The released cDNA before and after each laser stimulation (three ON/OFF laser pulses with 10 min ON duration and 30 min OFF) was quantified with the FAM fluorescence (Figure 3a). The irradiation denatured duplex DNA, while release was inhibited when NIR light was OFF. The accumulation of release increases as the cycles of laser ON/OFF increases. Similarly, the release of Pt(IV) prodrugs and Dox was carried out from Pt(IV)−dsDNA−Au NRs and

dx.doi.org/10.1021/am5000905 | ACS Appl. Mater. Interfaces 2014, 6, 4382−4393

Dox−dsDNA−Au NRs, respectively, in the same control manner (Figure 3b,c).

In Vitro Confocal Cells Imaging. Before the optical analysis, concentration dependent cell toxicity of FA−Pt(IV)/Dox−dsDNA−Au NRs was measured without laser irradiation (Figure S9, Supporting Information). For the further studies to balance the nontoxicity and the therapeutic effect after the laser irradiation, 200 ppm was selected as an optimal concentration. For in vitro studies, a confocal microscope was used to collect the fluorescence image and examine the cells cytotoxicity upon NIR laser irradiation. The malignant HeLa human cervical epithelial carcinoma cells (folate receptor positive)[31] were used for the intracellular targeting of FA−Pt(IV)/Dox−dsDNA−Au NRs, which have the hydrodynamic diameter of ∼88 ± 7 nm determined by DLS. As seen in Figures S7 and S8 (Supporting Information), the elevation of the temperature depends on the particle concentration and laser intensity. We have fixed 200 ppm (based on the Au ion concentration) for particle concentration and varied laser illumination with low intensity of 1.3 W/cm^2 (showing a solution temperature of around 45 °C after 10 min of exposure in Figure S8 (Supporting Information)) and higher 3 W/cm^2 (showing a solution temperature of up to 60 °C after 10 min of exposure in Figure S8 (Supporting Information)). The HeLa cells were incubated with 200 ppm nanomaterials at 37 °C. Then the cells were washed with PBS and laser irradiated at different laser densities. Herein, the red fluorescence of Dox provides an indicator for monitoring drug release. The cell membrane was stained with Alexa 488 to show green fluorescence and the nucleus was stained with DAPI to reveal blue fluorescence. For the image of the cells without laser treatment, there was a trace amount of Dox released after 2 h of incubation (Figure 4a). On the contrary, more red fluorescence from the released Dox appeared in the cytoplasm when the cells were exposed to 1.3 W/cm^2 of 808 nm diode laser after 2 h of incubation (Figure 4b). Because the fluorescence of Dox was quenched in the FA−Pt(IV)/Dox−dsDNA−Au NRs, the observation of the red fluorescence was contributed by the NIR-triggered "turn-on" of Dox fluorescence through the escape of Dox from DNA assembled on the NRs. Following the procedure of Figure 4b with the additional 24 h incubation resulted in a large amount release of Dox as well as of Pt(IV) prodrug, which caused severe damage to the nucleus that lead to the hazy DAPI image (Figure 4c). The representative cells with intact and hazy nucleus were indicated with the arrows in Figure 4b,c, respectively. Dox accumulation in the nuclei is apparent, when the cells were incubated for another 24 h. If we increased laser intensity to 3 W/cm^2 for the condition of Figure 4b, more Dox release was observed than that seen in Figure 4b (Figure 4d). The fluorescence image showed the laser intensity dependent increase in the red fluorescence, which is due to the enhanced Dox drug release with the increase in the laser intensity. Additionally, we observed severe cell membrane damage, marked with white arrows, due to the hyperthermia effect. If the cells, taken by following the procedure of Figure 4d, were further incubated for 24h, image shows the complete destruction of the cell morphology leading to severe reduction in the cell population (Figure 4e).

Evaluation of Cytotoxicity Using MTT Assay. MTT assay was used to evaluate cell viability. HeLa cells grown on 96-well plates were incubated with the 200 ppm (based on the Au ion concentration) of nanomaterials or free drugs for 2 h. Then the uninternalized nanomaterials or free drugs were removed and washed with PBS. For laser treatment, immediately after removing and washing with PBS, fresh medium was added and the cells were exposed to 10 min of 808 nm diode laser. In the case of the three laser treatment, 3 W/cm^2 laser followed three cycles of ON/OFF laser pulses with 10 min ON duration and 30 min OFF. Subsequently, the cells with or without the laser treatment were incubated for another 24 h at 37 °C before the MTT measurement. All of the nanomaterials were conjugated with FA to achieve HeLa cells targeting. For the groups of dsDNA−Au NRs and Dox−dsDNA−Au NRs, HOOC−PEG−COOH (MW: 2000) was conjugated with dsDNA with −COOH outward to form an amide link with the amine group of FA, leading to FA−HOOC−PEG−COOH−dsDNA−Au NRs and FA−HOOC−PEG−COOH−Dox−dsDNA−Au NRs. MTT results shown in Figure 5 indicate that the free drugs using Dox alone or Pt(IV) prodrug alone did not provide apparent cytotoxicity, giving 81% and 97% viabilities. On the other hand, the combined drugs (Pt(IV)+Dox) led to a certain degree of chemotherapeutic effect, resulting in a 72% cell viability. The dosage corresponds to 0.16 μM for free Pt(IV) and 1.6 μM for free Dox that are same amount carried by 200 ppm of Au NRs (∼4.6 mg Dox and ∼0.4 mg Pt(IV) per g of FA−Pt(IV)/Dox−dsDNA−Au NRs). In the absence of laser irradiation, FA−HOOC−PEG−COOH−dsDNA−Au NRs incubated with cells showed more than 90% cell viability, which indicated that the nanomaterial without the drug was biocompatible. The FA−Pt(IV)/Dox−dsDNA−Au NRs without laser exposure showed some toxic effect with a viability of 82%, probably due to the partial drug release from the loaded DNA in the condition inside the cells. Next, we examined toxicity upon NIR irradiation when the cells treated with nanomaterials. When the nondrug platform (FA−HOOC−PEG−COOH−dsDNA−Au NRs) was exposed to 3 W/cm^2 of laser intensity, a 75% cell viability was obtained, which is the exclusive effect of hyperthermia. Further, to understand the effect of the single drug carried by Au NRs exposed to the laser, the cells that were separately incubated with FA−HOOC−PEG−COOH−Dox−dsDNA−Au NRs and FA−Pt(IV)−dsDNA−Au NRs resulted in 61% and 73% cell viabilities. This difference in cell viability from these two nanocarriers can be explained in terms of the amount of Dox (1.6 μM) loading moreso than the Pt(IV) prodrug (0.16 μM) loading. As compared to the pure hyperthermia consequence (75% viability) using FA−HOOC−PEG−COOH−dsDNA−Au NRs, the Pt(IV) prodrug (73% viability) seems to not give an effective chemotherapeutic effect. The amount of Pt(IV) prodrug might be too small to show chemotherapy effects. However, for the cells incubated with FA−Pt (IV)/Dox−dsDNA−Au NRs exposed to the laser, the cell viability dropped to ∼50%. The combination of Pt(IV) prodrug and Dox led to an apparent chemotherapy than did the single drug carried by Au NRs. The exclusive additive chemotherapeutic effect of FA−Pt(IV)/Dox−dsDNA−Au NRs was calculated by $P_{additive} = (fA \times fB)\ P_0$,[32−34] where $P_{additive}$ is the final additive population, fA is cell viability after chemotherapy of FA−HOOC−PEG−COOH−Dox−dsDNA−Au NRs, fB is cell viability after chemotherapy of FA−Pt(IV)−dsDNA−Au NRs, and P_0 is the initial population. As mentioned in the aforementioned result, the nondrug platform (FA−HOOC−PEG−COOH−dsDNA−Au NRs), giving the exclusive effect of hyperthermia, resulted in a 75% cell viability. Herein, we excluded the hyperthermia effect exerted on the chemotherapy[33,35−38] by adding 25% cell viability to the

respective fA and fB. As a consequence, fA was 86% (61% + 25%) and fB was 98% (73% + 25%). According to this calculation, the theoretical additive effect ($P_{additive}$) was 84%. However, experimentally, the combination of Dox and Pt(IV) carried by Au NRs was determined as 75% (by addition of 25% with 50%). Hence, this enhancement in therapeutic behavior of our design experimentally over the theoretical additive effect is due to the synergistic effect of the drug combination. This combination effect is also reflected in the free drug combination. Interestingly, drugs carried by NRs revealed more effective therapeutic efficacy. If we conducted three cycles of ON/OFF laser pulses with 10 min ON duration and 30 min OFF, the viability further decreased to 42%. When the laser irradiation sequence was performed for 3 times, the hyperthermia toxicity from NRs (FA−HOOC−PEG−COOH−dsDNA−Au NRs) caused a 60% viability.

In Vivo Therapeutic Efficacy and Toxic Evaluation. We further evaluated the efficacy of the FA−Pt (IV)/Dox−dsDNA−Au NRs as an in vivo chemotherapeutic agent. The tumor growth was monitored in terms of tumor volume changes (Figure 6a). The xenografted mouse tumor model was established by sub-dermal injection of HeLa cancer cells. Thirty mice bearing tumors (~47 mm^3) were divided into six groups of control PBS, PBS + laser, free drugs (Pt(IV) + Dox), FA−Pt (IV)/Dox−dsDNA−Au NRs (nil laser irradiation), FA−HOOC−PEG−COOH−dsDNA−Au NRs + laser, and FA−Pt (IV)/Dox−dsDNA−Au NRs + laser. Because the in vitro results clearly showed that the combination of Pt(IV) prodrug and Dox led to apparent chemotherapy than the single drug treatment, we did not conduct experimental groups with single drug treatments (i.e., Dox, Pt(IV), FA−HOOC−PEG−COOH−Dox−dsDNA−Au NRs, FA−Pt(IV)−dsDNA−Au NRs, FA−HOOC−PEG−COOH−Dox−dsDNA−Au NRs + laser, FA−Pt(IV)−dsDNA−Au NRs + laser) for in vivo comparison. The mice injected with FA−Pt(IV)/Dox−dsDNA−Au NRs with drug amounts correspond to a dosage of 2 mg DOX/Kg and of 0.2 mg Pt(IV)/Kg through the tail vein. For the treatment with free drugs, the same amount of both drugs carried by Au NRs was injected intravenously. For the treatments with the laser, the tumors were irradiated by an 808 nm diode laser with an intensity of 3 W/cm^2 for 10 min after 2 h of materials injection. The P value was 0.03 at 14 days between the groups with free drugs (Pt(IV) + Dox) and FA−Pt(IV)−dsDNA−Au NRs + laser, showing statistical significance. Although a trend in the gradual increase in tumor size was observed, we have seen that the treatment with free drugs (Pt(IV) + Dox) revealed a certain degree of inhibition with delay growth in tumor. In the mice treated with hyperthermia alone (FA−HOOC−PEG−COOH−dsDNA−Au NRs + laser), the tumor size was inhibited at the initial 2 days, and then began to grow as days prolonged. The group injected with FA−Pt(IV)/Dox−dsDNA−Au NRs exposed to the laser displayed a slight decrease in tumor size, but the tumors were not suppressed. Continuous observation for up to 14 days showed no sign of tumor re-growth and tumor size remained constant throughout the observation period. When compared to the group treated with PBS, where the tumor grew steadily, the FA−Pt (IV)/Dox−dsDNA−Au NRs + laser revealed significant therapeutic efficacy (P value: 0.001). Figure 6b shows the biodistribution after injection of FA−Pt(IV)/Dox−dsDNA−Au NRs through the tail vein into mice bearing HeLa tumors. The tissues were surgically removed after 3 and 24 h of injection and analyzed. Tumors revealed dominant accumulation at both the intervals that supported the targeting effectiveness of FA−Pt(IV)/Dox−dsDNA−Au NRs. The excretion of NRs can be seen with the increase in the faeces at 24 h.

For the toxic evaluation of the as-prepared Pt(IV)/Dox−dsDNA−Au NRs, the long term effect of Pt(IV)/Dox−dsDNA−Au NRs on healthy mice without tumors was evaluated through tail vein injection at the Dox dosage of 2 mg/kg. In this long term observation, all the mice (n = 7) stayed alive for the experimental period of 21 days. Throughout the observation period, we did not encounter any mice death, hence a 100% mice survival was observed. The behavior of the mice was monitored every day and their weight was recorded periodically for 3 weeks and is shown in Figure 7a. For the weight comparison, the control set was injected with equal volume of PBS. Both sets of mice exhibited normal healthy behaviors without any symptoms of fatigue or changes in fur color or significant weight changes. In fact, the mice from both sets increased weight slightly at the end of 3 weeks. At the end of the long term observation, the mice were sacrificed and the histology of heart, lung, liver, kidney, and spleen tissue was examined for any change in the morphology due to material toxicity. The tissues after hematoxyline and eosin staining showed well-organized cell structure as that of the control set (Figure 7b). Especially the intact morphology of spleen, which plays an important role in blood purification, did not show any change in morphology due to absence of immune activity.

CONCLUSIONS

In summary, we reported the inorganic Au nanoplatform to achieve remote-controlled delivery of combined chemotherapy by carrying Dox and cisplatin prodrugs. The DNA duplexes tethered to Au NRs were loaded with Dox and cisplatin prodrugs to serve as an effective drug carrier to perform photothermal hyperthermia and dual drug release. The drugs were released with the NIR-laser stimulation, through the dehybridization of the duplex DNA, which caused significant cell toxicity in vitro. In vivo studies also showed the FA−Pt(IV)/Dox−dsDNA−Au NRs with the laser assistance effectively controlling the solid tumor growth in the mice model.

ASSOCIATED CONTENT

Supporting Information

Characterization of cisplatin prodrug; UV−vis, TEM and photothermal property of Pt(IV)/Dox-dsDNA-Au NRs; Dox flourescence. This material is available free of charge via the Internet at http://pubs.acs.org.

AUTHOR INFORMATION

Corresponding Authors

*C.-S. Yeh. E-mail: csyeh@mail.ncku.edu.tw.
*H.-F. Hsu. E-mail: konopka@mail.ncku.edu.tw.

Author Contributions

‖These authors contributed equally to the work.

Notes

The authors declare no competing financial interest.

ACKNOWLEDGMENTS

This work was supported by the National Science Council, Taiwan (NSC 101-2113-M-006-004-MY2)

REFERENCES

(1) Jia, J.; Zhu, F.; Ma, X.; Cao, Z. W.; Li, Y. X.; Chen, Y. Z. Mechanisms of Drug Combinations: Interaction and Network Perspectives. *Nat. Rev. Drug Discovery* **2009**, *8*, 111−128.

(2) Lehár, J.; Krueger, A. S.; Avery, W.; Heilbut, A. M.; Johansen, L. M.; Price, E. R.; Rickles, R. J.; Short, G. F.; Staunton, J. E.; Jin, X.; Lee, M. S.; Zimmermann, G. R.; Borisy, A. A. Synergistic Drug Combinations Tend to Improve Therapeutically Relevant Selectivity. *Nat. Biotechnol.* **2009**, *27*, 659−666.

(3) Lee, J.; Park, J. O.; Kim, W. S.; Park, S. H.; Park, K. W.; Choi, M. S.; Lee, J. H.; Koh, K. C.; Paik, S. W.; Yoo, B. C.; Joh, J.; Kim, K.; Jung, C. W.; Park, Y. S.; Im, Y.-H.; Kang, W. K.; Lee, M. H.; Park, K. Phase II Study of Doxorubicin and Cisplatin in Patients with Metastatic Hepatocellular Carcinoma. *Cancer Chemother. Pharmacol.* **2004**, *54*, 385−390.

(4) Thigpen, J. T.; Brady, M. F.; Homesley, H. D.; Malfetano, J.; DuBeshter, B.; Burger, R. A.; Liao, S. Phase III Trial of Doxorubicin With or Without Cisplatin in Advanced Endometrial Carcinoma: A Gynecologic Oncology Group Study. *J. Clin. Oncol.* **2004**, *22*, 3902−3908.

(5) Aapro, M. S.; van Wijk, F. H.; Bolis, G.; Chevallier, B.; van der Burg, M. E. L.; Poveda, A.; de Oliveira, C. F.; Tumolo, S.; Scotto di Palumbo, V.; Piccart, M.; Franchi, M.; Zanaboni, F.; Lacave, A. J.; Fontanelli, R.; Favalli, G.; Zola, P.; Guastalla, J. P.; Rosso, R.; Marth, C.; Nooij, M.; Presti, M.; Scarabelli, C.; Splinter, T. A. W.; Ploch, E.; Beex, L. V. A.; Huinink, W. B.; Forni, M.; Melpignano, M.; Blake, P.; Kerbrat, P.; Mendiola, C.; Cervantes, A. A.; Goupil; Harper, P. G.; Madronal, C.; Namer, M.; Scarfone, G.; Stoot, J. E. G. M.; Teodorovic, I.; Coens, C.; Vergote, I.; Vermorken, J. B. Doxorubicin Versus Doxorubicin and Cisplatin in Endometrial Carcinoma: Definitive Results of a Randomised Study (55872) by the EORTC Gynaecological Cancer Group. *Ann. Oncol.* **2003**, *14*, 441−448.

(6) Nielsen, D.; Larsen, P. D. S. K.; Skovsgaard, O. P. H. T. Epirubicin or Epirubicin and Cisplatin as First-Line Therapy in Advanced Breast Cancer. A phase III study. *Cancer Chemother. Pharmacol.* **2000**, *46*, 459−466.

(7) Martoni, A.; Bellucco, A.; Canova, N.; Pannuti, F. Four-Year Analysis of Platinum and Anthracycline Combination for Ovarian Cancer. *Oncology* **1989**, *46*, 109−116.

(8) Wang, X.; Liu, Q.; Hou, B.; Zhang, W.; Yan, M.; Jia, H.; Li, H.; Yan, D.; Zheng, F.; Ding, W.; Yi, C.; Wang, H. Concomitant Targeting of Multiple Key Transcription Factors Effectively Disrupts Cancer Stem Cells Enriched in Side Population of Human Pancreatic Cancer Cells. *PLoS One* **2013**, *8*, e73942.

(9) Hu, C. M.; Aryal, S.; Zhang, L. F. Nanoparticle-Assisted Combination Therapies for Effective Cancer Treatment. *Ther. Delivery* **2010**, *1*, 323−334.

(10) Davis, M. E.; Chen, Z.; Shin, D. M. Nanoparticle Therapeutics: an Emerging Treatment Modality for Cancer. *Nat. Rev. Drug Discovery* **2008**, *7*, 771−782.

(11) Peer, D.; Karp, J. M.; Hong, S.; Farokhzad, O. C.; Margalit, R.; Langer, R. Nanocarriers as an Emerging Platform for Cancer Therapy. *Nat. Nanotechnol.* **2007**, *2*, 751−760.

(12) Lee, S.-M.; O'Halloran, T. V.; Nguyen, S. B. T. Polymer-Caged Nanobins for Synergistic Cisplatin−Doxorubicin Combination Chemotherapy. *J. Am. Chem. Soc.* **2010**, *132*, 17130−17138.

(13) Kolishettia, N.; Dharc, S.; Valenciad, P. M.; Lind, L. Q.; Karnike, R.; Lippard, S. J.; Langer, R.; Farokhzad, O. C. Engineering of Self-Assembled Nanoparticle Platform For Precisely Controlled Combination Drug Therapy. *Proc. Natl. Acad. Sci. U. S. A.* **2010**, *107*, 17939−17944.

(14) Shuhendler, A. J.; Cheung, R. Y.; Manias, J.; Connor, A.; Rauth, A. M.; Wu, X. Y. A Novel Doxorubicin-Mitomycin C Co-encapsulated Nanoparticle Formulation Exhibits Anti-Cancer Synergy in Multidrug Resistant Human Breast Cancer Cells. *Breast Cancer Res. Treat.* **2010**, *119*, 255−269.

(15) Wang, H.; Zhao, Y.; Wu, Y.; Hu, Y. L.; Nan, K.; Nie, G.; Chen, H. Enhanced Anti-Tumor Efficacy By Co-Delivery Of Doxorubicinand Paclitaxel With Amphiphilic Methoxy PEG-PLGA Copolymer Nanoparticles. *Biomaterials* **2011**, *32*, 8281−8290.

(16) Singh, A.; Dilnawaz, F.; Mewar, S.; Sharma, U.; Jagannathan, N. R.; Sahoo, S. K. Composite Polymeric Magnetic Nanoparticles for Co-Delivery of Hydrophobic and Hydrophilic Anticancer Drugs and MRI Imaging for Cancer Therapy. *ACS Appl. Mater. Interfaces* **2011**, *3*, 842−856.

(17) Kim, D.; Jeong, Y. Y.; Jon, S. A Drug-Loaded Aptamer−Gold Nanoparticle Bioconjugate for Combined CT Imaging and Therapy of Prostate Cancer. *ACS Nano* **2010**, *4*, 3689−3696.

(18) Bagalkot, V.; Farokhzad, O. C.; Langer, R.; Jon, S. An Aptamer−Doxorubicin Physical Conjugate as a Novel Targeted Drug-Delivery Platform. *Angew. Chem., Int. Ed.* **2006**, *45*, 8149−8152.

(19) Frederick, C. A.; Williams, L. D.; Ughetto, G.; van der Mare1, G. A.; van Boom, J. H.; Rich, A.; Wang, A. H. Structural Comparison of Anticancer Drug-DNA Complexes: Adriamycin and Daunomycin. *Biochemistry* **1990**, *29*, 2538−2549.

(20) Hurst, S. J.; Lytton-Jean, A. K. R.; Mirkin, C. A. Maximizing DNA Loading on a Range of Gold Nanoparticle Sizes. *Anal. Chem. (Washington, DC, U. S.)* **2006**, *78*, 8313−8318.

(21) Demers, L. M.; Mirkin, C. A.; Mucic, R. C.; Reynolds, R. A.; Letsinger, R. L.; Elghanian, R.; Viswanadham, G. A Fluorescence-Based Method for Determining the Surface Coverage and Hybridization Efficiency of Thiol-Capped Oligonucleotides Bound to Gold Thin Films and Nanoparticles. *Anal. Chem. (Washington, DC, U. S.)* **2000**, *72*, 5535−5541.

(22) Barnes, K. R.; Kutikov, A.; Lippard, S. Synthesis, characterization, and cytotoxicity of a series of estrogen-tethered platinum(IV) complexes. *Chem. Biol.* **2004**, *11*, 557−564.

(23) Yang, J.; Liu, W.; Sui, M.; Tang, J.; Shen, Y. Platinum (IV)-Coordinate Polymers as Intracellular Reduction-Responsive Backbone-Type Conjugates for Cancer Drug Delivery. *Biomaterials* **2011**, *32*, 9136−9143.

(24) Jana, N. R.; Gearheart, L.; Murphy, C. J. Wet Chemical Synthesis of High Aspect Ratio Cylindrical Gold Nanorods. *J. Phys. Chem. B* **2001**, *105*, 4065−4067.

(25) Dhar, S.; Daniel, W. L.; Giljohann, D. A.; Mirkin, C. A.; Lippard, S. J. Polyvalent Oligonucleotide Gold Nanoparticle Conjugates as Delivery Vehicles for Platinum(IV) Warheads. *J. Am. Chem. Soc.* **2009**, *131*, 14652−14653.

(26) Wang, S.; Lee, R. J.; Mathias, C. J.; Green, M. A.; Low, P. S. Synthesis, Purification, and Tumor Cell Uptake of ^{67}Ga-Deferoxamine−Folate, a Potential Radiopharmaceutical for Tumor Imaging. *Bioconjugate Chem.* **1996**, *7*, 56−62.

(27) Martínez, R.; García, L.C. The Search of DNA-Intercalators as Antitumoral Drugs: What it Worked and What did not Work. *Curr. Med. Chem.* **2005**, *12*, 127−151.

(28) Ihmels, H.; Otto, D. Intercalation of Organic Dye Molecules into Double-stranded DNA. Part 1: The Annelated Quinolizinium Ion as a Structural Motif in DNA Intercalators. *Top. Curr. Chem.* **2005**, *258*, 161−204.

(29) Cashman, D. J.; Scarsdale, J. N.; Kellogg, G. E. Hydropathic Analysis of the Free Energy Differences in Anthracycline Antibiotic Binding to DNA. *Nucleic Acids Res.* **2003**, *31*, 4410−4416.

(30) Huschka, R.; Zuloaga, J.; Knight, M. W.; Brown, L. V.; Nordlander, P.; Halas, N. J. Light-Induced Release of DNA from Gold Nanoparticles: Nanoshells and Nanorods. *J. Am. Chem. Soc.* **2011**, *133*, 12247−12255.

(31) Santra, S.; Jativa, S. D.; Kaittanis, C.; Normand, G.; Grimm, J.; Perez, J. M. Gadolinium-Encapsulating Iron Oxide Nanoprobe as Activatable NMR/MRI Contrast Agent. *ACS Nano* **2012**, *6*, 7281−7294.

(32) Kuo, W. S.; Chang, C. N.; Chang, Y. T.; Yeh, C. S. Antimicrobial Gold Nanorods with Dual-Modality Photodynamic Inactivation and Hyperthermia. *Chem. Commun.* **2009**, *45*, 4853−4855.

(33) Hauck, T. S.; Jennings, T. L.; Yatsenko, T.; Kumaradas, J. C.; Chan, W. C. W. Enhancing the Toxicity of Cancer Chemotherapeutics with Gold Nanorod Hyperthermia. *Adv. Mater.* **2008**, *20*, 3832−3838.

(34) Hahn, G. M.; Braun, J.; Har-Kedar, I. Thermochemotherapy: Synergism Between Hyperthermia (42-43 degrees) and Adriamycin (of Bleomycin) in Mammalian Cell Inactivation. *Proc. Natl. Acad. Sci. U. S. A.* **1975**, *72*, 937−940.
(35) Liu, H. Y.; Chen, D.; Li, L. L.; Liu, T. L.; Tan, L. F.; Wu, X. L.; Tang, F. Q. Multifunctional Gold Nanoshells on Silica Nanorattle: A Novel Potential Platform for Combination of Photothermal Therapy and Chemotherapy with Low Systemic Toxicity. *Angew. Chem., Int. Ed.* **2011**, *50*, 891−895.
(36) Lee, S. M.; Park, H.; Yoo, K. H. Synergistic Cancer Therapeutic Effects of Locally Delivered Drug and Heat Using Multifunctional Nanoparticles. *Adv. Mater.* **2010**, *22*, 4049−4053.
(37) Bull, J. M. C. An Update on the Anticancer Effects of a Combination of Chemotherapy and Hyperthermia. *Cancer Res.* **1984**, *44*, 4853−4856.
(38) Palzer, R. J.; Heidelberger, C. Influence of Drugs and Synchrony on the Hyperthermic Killing of HeLa Cells. *Cancer Res.* **1973**, *33*, 422−427.